Construction of a Compact Two-Dimensional Magneto-Optical Trap for a Cold Calcium Beam

Daniel C. Woodbury

A senior thesis submitted to the faculty of
Brigham Young University
in partial fulfillment of the requirements for the degree of

Bachelor of Science

Scott D. Bergeson, Advisor

Department of Physics and Astronomy

Brigham Young University

April 2015

ABSTRACT

Construction of a Compact Two-Dimensional Magneto-Optical Trap
for a Cold Calcium Beam

Daniel C. Woodbury
Department of Physics and Astronomy, BYU
Bachelor of Science

We present the construction and characterization of a two-dimensional magneto-optical trap (MOT) as a source of cold calcium atoms. Atoms are cooled transversely from a hot effusive source and captured in the 2-D MOT without axial confinement. We present calculations for and creation of the calcium source, as well as calculations for a paired ytterbium 2-D MOT. The results demonstrate that the 2-D MOT is feasible for calcium, with atomic density reaching a peak of 1.3×10^9 atoms/cm^3 in the trap. While we predict these densities can provide a loading rate 25 times higher than loading directly from an effusive beam, we were not able to successfully create a 3-D MOT. We present possible reasons for these results, as well as our future plans for experimental development.

Keywords: magneto-optical trap, cold atom sources, ultracold plasma

ACKNOWLEDGMENTS

I would like to acknowledge Dr. Bergeson for his inspiration and mentoring, as well as Alex Erikson, who helped me with work on this project. I would also like to acknowledge personal funding from both the BYU Physics Department and the BYU Office of Research and Creative Activities.

This work supported in part by the NSF (Grant No. PHY-0969856) and the Air Force (Grant No. FA9950-12-1-0308).

Contents

List of Figures

Chapter 1

Introduction

Cold atomic beam sources are fundamental for trapping and studying ultracold gases, collections of atoms with temperatures in the μK range. These ultracold gases provide a regime for studying many-body quantum physics, strongly correlated systems, and other fundamental processes [1]. Advances in the study of cold atoms have created a constant need for improvements in cooling and trapping atoms. To this end, we have built a source for a high-flux cold calcium beam to use in our study of ultracold neutral plasma, replacing a less efficient method from our past experiments.

Section 1.1 details the motivation for our work in ultracold neutral plasma. Sections 1.2 and 1.3 review the basics of laser cooling and trapping. Sections 1.4 and 1.5 detail our novel beam source, while an overview of the remainder of the thesis is given in Sec. 1.6.

1.1 Ultracold Neutral Plasma

Scientists study ultracold neutral plasmas to better understand more complicated systems, since they provide an easily accessible platform for studying non-ideal plasmas [2]. In particular, ultracold plasmas exhibit strong coupling, a state in which the average potential energy due to Coulomb interactions exceeds a particle's average kinetic energy. Plasmas that share this same ratio of po-

tential energy to kinetic energy exhibit similar behavior, even if they have disparate temperatures and densities. Hence ultracold neutral plasmas provide an important analogue to hot dense plasma and strongly coupled systems in general.

A dual-species ultracold plasma potentially provides insight on transport mechanisms in fusion-class plasmas. Scientists do not fully understand ion-electron energy transport in dense plasma, but efficient energy transport between hot electrons and the ions is necessary for sustained fusion burn. Since magnetized electron and ion plasmas have widely disparate time scales, complete and detailed computer simulations of the underlying physical processes are challenging. Similar interactions in ultracold plasma are easier to observe using high precision spectroscopy. Bannasch et al. already demonstrated such an approach to energy relaxation in a single-species ultracold plasma by tracking the velocity profiles of the ions [3]. Two atomic species of different masses provide a more refined system for studying energy relaxation, since the two different species provide an analogue to ions and electrons. Since the mass ratio between calcium and ytterbium is 500 times smaller than that for protons and electrons, we can more easily use computational methods to understand and interpret our experimental results. With this goal in mind, we built a new experimental chamber for a dual-species plasma consisting of calcium and ytterbium. This thesis addresses the cooling and trapping of calcium as a first step in this project.

1.2 Laser Cooling

A two-level atom in resonance with a laser field absorbs photons and sees a force from the resulting transfer of momentum, as represented by Fig. 1.1. In subsequent interactions, stimulated emission will simply reverse this momentum transfer. Spontaneous emission, however, releases photons in all directions and over many individual events results in no net change in momentum. Spontaneous emission occurs with a frequency given by the inverse of the excited state lifetime, or $\Gamma = 1/\tau$. As

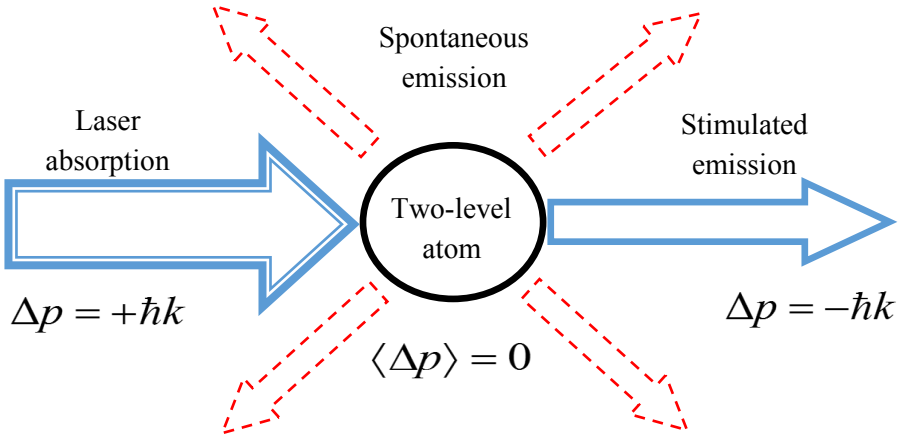

Figure 1.1 When a two-level atom propagating against laser light absorbs a photon, it receives a momentum "kick" and the atom is slowed. While stimulated emission reverses this effect, spontaneous emission—on average—does not. Hence the atom sees an effective force over many cycles of absorption and emission. In the figure, $\hbar k$ is the momentum associated with each photon.

Metcalf and van der Straten showed in their seminal work [4], the force a resonant laser beam in terms of Γ, the laser's wavenumber k, and the laser saturation $s_0 = I/I_0$ is

$$F = \hbar k \Gamma \frac{s_0/2}{1+s_0}. \tag{1.1}$$

If we inspect this equation, we find that the first factor, $\hbar k\Gamma$, is simply the amount of momentum transferred for each absorbed photon times the average frequency of spontaneous emission. The second term is the probability that an atom will be found in the excited state, and accounts for stimulated emission. For high intensities, this factor saturates to $1/2$, corresponding to atoms constantly being pumped between the ground and excited states. With these considerations in mind, the maximum force which an atom experiences in a laser field is $F = \hbar k\Gamma/2$.

When a laser beam is out of resonance with the atom, we must modify the above equation to account for the decreased interaction [4]. Non-resonance stems both from laser detuning, where the laser frequency is separated from the atomic transition by an amount δ_L, and from a Doppler shift, since atoms moving with velocity $\vec{v}$ in laser light with wavevector $\vec{k}$ will see a frequency shift

$\omega_D = \vec{v} \cdot \vec{k}$. Adding all such effects together, we arrive at an effective detuning $\delta_{eff} = \delta_L + \omega_D$. Taking this into account, we can rewrite Eq. (1.1) away from resonance as

$$F = \frac{\hbar k s_0 \Gamma/2}{1 + s_0 + (2\delta_{eff}/\Gamma)^2}. \tag{1.2}$$

From the equation we see that the force on the atoms decreases as it moves farther from resonance, with a width related to Γ.

Without external fields or high intensities, a resonant laser beam will exert a force on an atom and accelerate until it is out of resonance, which for calcium corresponds to a change in velocity of only ~15 m/s. To successfully cool an atom, we must change the effective detuning to match the acceleration of the atom. Early pioneers in laser cooling actually used chirped laser systems to change the laser frequency as the atom slowed [4]. This method inherently produces a pulsed atomic beam, so most scientists now use magnetic fields to provide the necessary change in detuning. The Zeeman shift $\Delta E = m_j \mu_B B$ describes the shift in energy for an atomic level with magnetic quantum number m_j, where μ_B is the Bohr magneton and B is the external magnetic field. By matching a changing magnetic field with the deceleration of the atom, one can slow atoms over a wider velocity range.

1.3 Optical Trapping

A cold beam of atoms can easily be trapped in various optical setups. For sufficiently slow atoms, three retro-reflected, orthogonal beams tuned below resonance produce an "optical molasses" [4]. If an atom moves too quickly, it is Doppler shifted into resonance, and the resulting optical force slows it until it is no longer in resonance with the beam. This damping force, however, does not prevent atoms from slowly drifting out of the region, limiting the density of atoms in the region.

To confine atoms more stably, we must add a spatially dependent force. A quadrupole magnetic field, along with a specific polarization and laser detuning on each beam, provides this force and

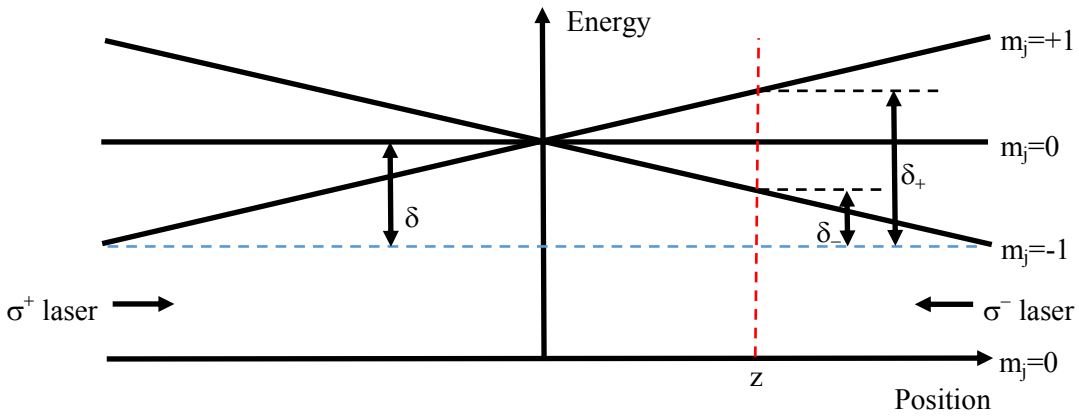

Figure 1.2 (color online) An energy diagram for atoms confined in the magneto-optical trap. Both lasers are detuned from resonance by an amount δ (energy of each photon indicated by the horizontal blue dotted line). As an atom strays from the trap center (origin) to a position z (vertical red dotted line), the magnetic field shifts its energy levels. Hence the atom will see the beam corresponding to the lowest transition closer to resonance than the beam corresponding to the other transition, which results in a net force towards the center of the trap.

turns the optical molasses into a stable magneto-optical trap (MOT) . A pair of anti-Helmholtz coils (carrying current in opposite directions) produce the quadrupole field, which is zero at the center of the trap. For small displacements in any direction from this spot, the magnitude of the magnetic field increases linearly. Figure 1.2 provides a schematic for the resulting split in excited state energy levels, whose magnitude is given by the Zeeman shift $\Delta E = m_j \mu_B B$. The opposing σ^+ (σ^-) circularly polarized beams excite atoms exclusively to the $m_j = 1(-1)$ states, respectively. As an atom drifts farther from the trap center, the atom sees transitions to the energy level corresponding to the anti-propagating laser beam closer to resonance, while the energy level corresponding to the co-propagating beam is shifted farther from resonance. As demonstrated in Eq. (1.2), the difference in detuning between the two beams results in a greater force from the anti-propagating beam, and the atom is pushed back towards the trap center.

The number of atoms loaded into the trap is limited by a capture velocity of the MOT, and

atoms exceeding this velocity will pass through the trapping region. At the roughest level, we can estimate this trapping velocity by assuming maximum deceleration of atoms over the radius of a MOT beam. For a calcium MOT with 1 cm diameter beams, this gives an estimate of $v_c \approx 90$ m/s. Since only a very small tail of a thermal distribution of atoms have velocities below the capture velocity, additional apparatus must prepare a source of cold atoms to effectively load a large number of atoms into the MOT.

1.4 Past Work in Trap Loading

There are a variety of methods to slow atoms and load them into 3-D MOTs, including effusive beam sources, Zeeman slowers, and vapor cell MOTs (VCMOTS). An effusive beam source with a paired slowing laser, while easy to implement for calcium, introduces hot background flux and only captures a few atoms. Zeeman slowers, which add a variable magnetic field to keep atoms from the oven source in resonance with the slowing beam, decrease some of the background flux and increase the capturable velocity range. However, they are large and unwieldy, and also require extensive windings to create a specific magnetic field configuration. Vapor cell MOTs are popular for atomic species with high vapor pressure. They actually allow one to load a MOT directly from background gas in the experimental chamber or to cool the atoms and then transfer them to a separate chamber. Calcium has a low vapor pressure at room temperature, eliminating the use of a VCMOT: insufficient amounts would be present in the cell to recapture at low temperature. If, on the other hand, calcium vapor is used at high temperature, the corrosive nature of calcium becomes an important consideration.

In the current experiment in our laboratory, a laser beam slows a small portion of atoms emitted from an effusive source so they can be captured in the MOT. This process fails to remove the hot background flux and complicates trap geometry, since the slowing beam can perturb the MOT if

aimed directly through its center. Additionally, only a small solid angle of the flux emitted from the oven can be captured in the MOT, reducing efficiency.

1.5 2-D MOT Concept for Trap Loading

A separate two-dimensional MOT placed in close proximity to the atomic oven provides an efficient alternative to these methods. Figure 1.3 shows a schematic of the 2-D MOT setup. Tiecke, et al. demonstrated in 2009 that this setup can provide a high-flux atomic beam for lithium, another alkali metal with characteristics similar to calcium, while achieving little background flux [5]. The mechanics of slowing and trapping is analogous to the three-dimensional case discussed in Sec. 1.3. The quadrupole magnetic field, however, has axial symmetry, and only two sets of counter propagating laser beams cool the atoms, allowing atoms to freely move along the axis of the trap. Only sufficiently cooled atoms are transferred into the main chamber, while high-velocity atoms that escape the 2-D MOT do not enter the chamber and do not contribute to background pressure there.

Although atoms can freely move into the main chamber and be recaptured, most do not have sufficient axial velocity and require a transfer mechanism. A laser push beam detuned below resonance facilitates the transfer of atoms from the 2-D MOT to the main experimental chamber. The beam accelerates atoms through a channel into the main chamber, but the atoms remain at a velocity low enough for recapture into the main MOT.

These advantages led us to use paired 2-D magneto-optical traps to load both calcium and ytterbium into the main chamber. Several other groups, including Tiecke's, used a 2-D MOT to load atoms into a dual-species MOT containing lithium and potassium [6, 7], while another group also used this method to load ytterbium into a conventional MOT [8]. Their success convinces us that a calcium and ytterbium MOT loaded from the 2-D MOTs is an attainable goal.

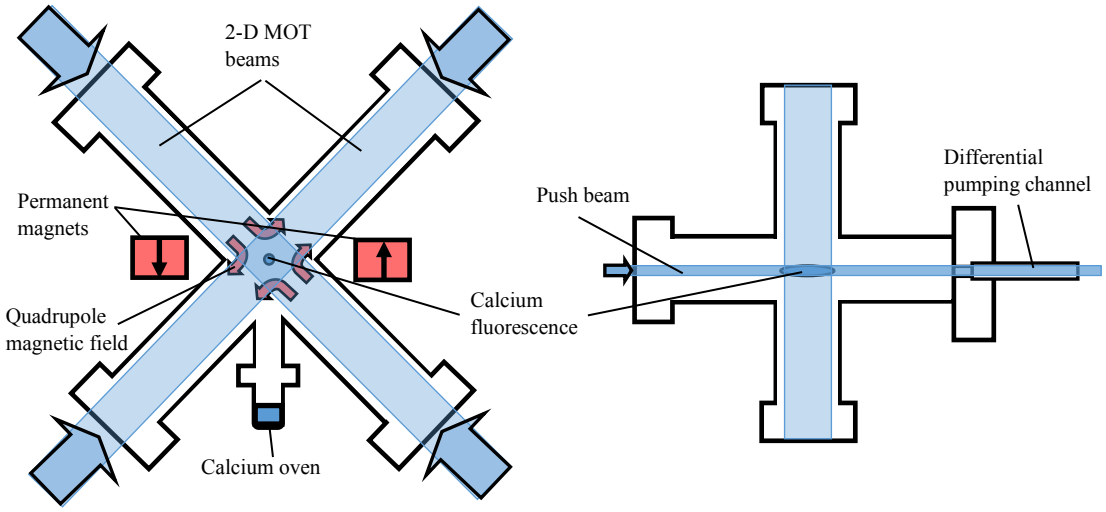

Figure 1.3 Schematic of 2-D MOT concept. Similar to a 3-D MOT, this system slows atoms emitted from an oven using counter-propagating lasers and a quadrupole magnetic field. A pair of permanent magnets provide a high field gradient, and a push beam accelerates atoms from the 2-D MOT into the main chamber.

1.6 Overview

My thesis outlines the construction and characterization of a 2-D magneto-optical trap (MOT) as a cold calcium source. In this process we address two questions: whether the 2-D MOT concept is functional for calcium, and whether the effective flux of cold atoms from the 2-D MOT exceeds previous loading methods in our lab. Currently we can create a MOT with about 2×10^7 atoms and would like to increase this number by at least an order of magnitude.

Chapter 2 explains the distinct systems in the experimental setup, including the vacuum chamber, atom source, magnetic field sources and data collection. Appendix A contains more detailed information about the electronics used to power the MOT field coils.

Chapter 3 details our results, trap parameters, and thoughts about future work. We observed a peak atomic density of 1.3×10^9 atoms/cm^3 in the 2-D MOT, which we calculate will support an atomic flux about 30 times better than our previous setup.

Chapter 2

Experimental Methods

The bulk of this chapter reviews the primary systems for creating our 2-D magneto-optical trap (MOT). Each of these systems is critical to the final setup, so we review each of them, along with necessary considerations for construction. We also present the diagnostic equipment used to optimize the MOT and measure its performance.

2.1 Extending Calculations from Lithium to Calcium

Tiecke et al. detailed a semi-empirical model for atom capture and loading in their paper, which we use to predict the efficiency of our experimental setup [5]. The model accounts for the total flux emitted from a thermal source, the number of atoms with velocities below the capture velocity of the 2-D MOT, and subsequent van der Waals interactions with background atomic flux.

When we replace the values for lithium with those for calcium, we find that expected results for calcium trapping are favorable. Repeating this process for a variety of elements to decide which species we could load along with the calcium in a dual-species MOT, we find that ytterbium is most promising, both in terms of cooling efficiency and in terms of the laser wavelengths needed for laser cooling. Sections 2.3 and 2.4 detail the relevant calculations from Tiecke's paper, along

with the updated values for calcium and ytterbium.

2.2 Vacuum Chamber

The vacuum system consists of three distinct chambers, with two identical 2-D MOT cells connected to each side of the main experimental chamber. A differential pumping (DP) channel between the 2-D MOT chambers and the main chamber reduces gas load in the main chamber. Each chamber is equipped with an ion pump, and gate valves allow separate servicing of the chambers. A total of 12 viewports allow optical access to the main chamber; four mini-viewports have Brewster windows, which we added to admit high power laser pulses.

We use a six-way cross for the 2-D MOT (refer to Fig. 1.3 for axial and side views), paralleling the implementation by Tiecke et al. The oven consists of a small tube welded on the bottom of the cross. Atoms emitted from the oven have no direct line of sight to the main chamber, eliminating background flux from the oven and maintaining low pressures for the 3-D MOT.

2.3 Magnetic Field Sources

The maximum field gradient $\partial B/\partial r$ in the 2-D MOT is limited by atomic characteristics, since atomic mass and linewidth dictate the deceleration of atoms in the laser field. As explained in Sec. 1.2, an atom achieves resonance with the slowing laser light when frequency shifts from the Zeeman shift and the Doppler shift match the laser detuning. Tiecke et al. used this fact to express the maximum velocity for which an atom will satisfy resonance in the 2-D MOT region as

$$\mathrm{v}_{\max} = \lambda_L \frac{\sqrt{2}}{2\pi}\left[\frac{\mu_B}{\hbar}\frac{\partial B}{\partial r} r_{\max} - \delta_L\right], \tag{2.1}$$

where $r_{\max}$ is the maximum distance for slowing, δ_L is the laser detuning, λ_L is the laser wavelength, μ_B is the Bohr magneton, and the factor of $\sqrt{2}$ accounts for the 45° angle between the

atomic flux and the MOT laser beams.

Since a laser beam can only provide a maximum deceleration force of $\hbar k\Gamma/2$ (refer to Sec. 1.2), the magnetic field cannot exceed a certain value for any given velocity and still match the atom's deceleration. Stipulating that the field gradient matches the change in the Doppler shift at maximum deceleration, Tiecke derives the constraint

$$v_{max} \leq \frac{\sqrt{1/8}(\hbar k)^2}{m\mu_B(\partial B/\partial r)}\Gamma. \tag{2.2}$$

By setting Eq. (2.1) and Eq. (2.2) equal to each other, assuming that $\delta_Z >> \delta_L$, and solving for the field gradient, we obtain the inequality

$$\frac{\partial B}{\partial r} \leq \frac{(\hbar k)^{3/2}}{2\mu_B(m r_{max})^{1/2}}\Gamma^{1/2}. \tag{2.3}$$

When we apply Eqs. (2.1)-(2.3) to calcium and ytterbium and insert the beam radius in our experiment ($r_{max} \approx 0.7$ cm), we find that the maximum field gradients are 2.28 T/m and 1.09 T/m for calcium and ytterbium, respectively. While these field gradients are higher than that in Tiecke's work (0.5 T/m), they represent an upper bound for which atoms will still be cooled the entire time they are in the trapping region. If the magnetic field gradients are below these values, atoms will still be cooled and trapped, but the 2-D MOT will have a lower capture velocity.

We can now substitute $\partial B/\partial r$ back into Eq. (2.1) or Eq. (2.2) to obtain the maximum velocity of atoms slowed by the lasers of the 2-D MOT. However, Tiecke notes that we cannot expect all atoms which undergo cooling to end up in the trap. Hence, we apply the same ratio between his calculated v_{max} and his observed capture velocity, $v_c = 0.85 v_{max}$, to estimate that our capture velocities will be about 110 m/s and 50 m/s for calcium and ytterbium.

To provide the high gradients needed in the 2-D quadrupole field, we use a pair of permanent magnets on each of the six-way crosses. We mount the magnets directly on the exterior of the MOT cross with a pair of brackets, which also ensure the magnets are level. Both sets of neodymium

rare earth magnets are from K & J Magnetics, the dimensions of those for the calcium MOT being 3"x1"x1/2" and those for the ytterbium MOT being 3"x1/2"x1/2".

For the main chamber, a pair of water cooled copper coils with 25 turns each provide the necessary magnetic field, and current is supplied with an 18 V 200 A power supply. The design of these coils is comparable to those on our older experiment, though they are slightly larger. When running, the coils produce a magnetic field gradient of about 70 G/cm (gauss/centimeter).

2.4 Calcium Oven

The calcium oven consists of a welded tube extending down from the six way cross, filled with solid calcium pellets under vacuum. An insulated external coil is driven by a PID controller to raise the calcium to temperatures of 450-550° C. At these temperatures, both calcium and ytterbium remain in a solid state, but gas partial pressure increases to produce a sizable atomic flux from the oven.

To model the flux in his calculations , Tiecke replaced the oven with an emissive source at the saturated vapor pressure of lithium, which led to the flux equation

$$\Phi_c = n_s A \int_0^{\Omega_c} d\Omega \frac{\cos\theta}{4\pi} \frac{1}{\mathscr{N}} \int_0^{v_c} v^3 e^{-(v/\alpha)^2} dv, \tag{2.4}$$

where n_s is the atomic density, A is the area over which the oven emits, Ω_c is the solid angle of the trapping region, θ is the emission angle, α is the most probable thermal speed and $\mathscr{N}$ is a normalization factor for the integral. Since our oven geometry resembles that in Tiecke's paper, we compare flux for different atomic species simply as a ratio of the integral over the velocity distribution. For $v_c << \alpha$, this integral is proportional to $(v_c/\alpha)^4$. By comparing these values, we find that calcium and ytterbium both produce high flux atomic sources at our oven temperature, exceeding flux from lithium and strontium by at least an order of magnitude.

Since we are only able to capture the tail of the velocity distribution, hot background flux will interact with slower atoms and possibly deflect them away from the 2-D MOT trapping region.

Tiecke described these "knock-out" collisions using a model of van der Waals interactions between atoms which deflect slow atoms outside the capture region [5]. These interactions result in an attenuation factor, $\exp[-n_s\bar{v}\sigma\tau]$, where σ and τ are the calculated collision cross section and characteristic time for van der Waals interactions outside the trap, while n and $\bar{v}$ are the density and average velocity of atoms. To compare knock-out between species, we take the attenuation factor which Tiecke reported and simply change the values of σ and τ for interactions outside the trap to roughly estimate attenuation. Compared to Tiecke's calculated attenuation factor of 0.27 (i.e. only 27% of capturable atoms making it to the 2-D MOT), we predict attenuation of only 0.68 and 0.70 for calcium and ytterbium.

2.5 Laser System

To provide laser light for the calcium 2-D MOT, we employ a frequency doubling cavity. We first drive a tunable diode laser to produce light at $\lambda = 846$ nm. We then focus the light in the center of a frequency doubling cavity with an lithium triborate (LBO) crystal, which produces light at $\lambda = 423$ nm, the cooling and trapping wavelength for calcium. Because there is no hyperfine structure for calcium's principal transition, we do not need any additional trapping lasers. A femtosecond frequency comb allows us to lock our infrared laser to the correct detuning [9]. Figure 2.1 gives a simplified schematic of the laser setup.

To apply different laser detuning to the 2-D MOT, 3-D MOT and probe beams, we use an acousto-optic modulator (AOM). We lock the main output of our laser at 80 MHz below resonance, a detuning which optimizes the 2-D MOT. We then use a 40 MHz AOM to create 3-D MOT beams tuned 40 MHz below resonance and a weak resonant probe beam.

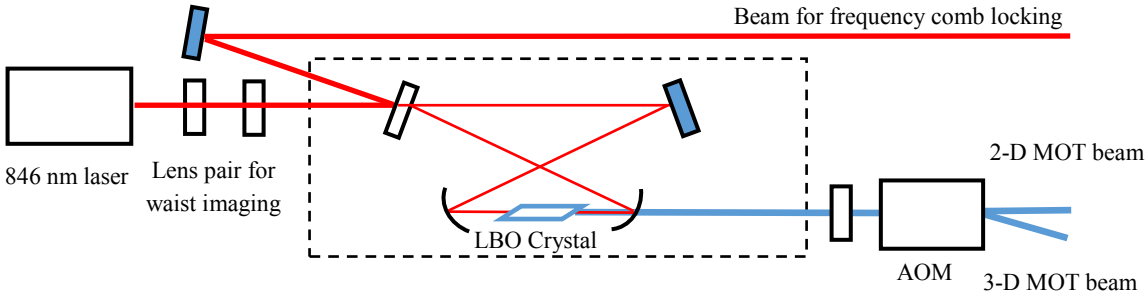

Figure 2.1 The 846 nm laser is focused to create a beam waist at the center of the top leg of the cavity. The mirrors then image this waist in the center of the LBO frequency doubling crystal. The output of the cavity is acoustically modulated to create distinct detuning on the MOT beams, while the remaining 846 nm light is used to lock the frequency to our femtosecond comb.

2.6 Elements for Precision Spectroscopy

Although we will primarily use the dual-species MOT to study ultracold plasma, we also plan to perform precision spectroscopy measurements on the elements in the trap. In order to eliminate shifts in measured energy levels, we needed to cancel all magnetic fields at the center of the main chamber. Three sets of Helmholtz coils cancel all bias fields, while several electronic components in the magnetic coil power lines enable quick switching of the MOT quadrupole field.

Any leftover magnetic fields in the chamber will introduce an energy shift in atomic transitions, given by $\Delta f = m_j \mu_B B$, where the Bohr magneton $\mu_B = 1.4$ MHz/G. Since we adjusted the Helmholtz coils to zero the magnetic field to ± 20 milligauss, we calculate uncertainty in frequency measurements caused by a magnetic field bias to be ± 30 kHz, well below uncertainty from other experimental considerations. To reduce errors from the MOT quadrupole field, we must turn off the field source and allow atoms to expand ballistically. After a few microseconds, the leftover magnetic field from the coils will introduce an additional uncertainty of about 70 kHz in the frequency measurements. Appendix A contains a detailed description of the power switching electronics for

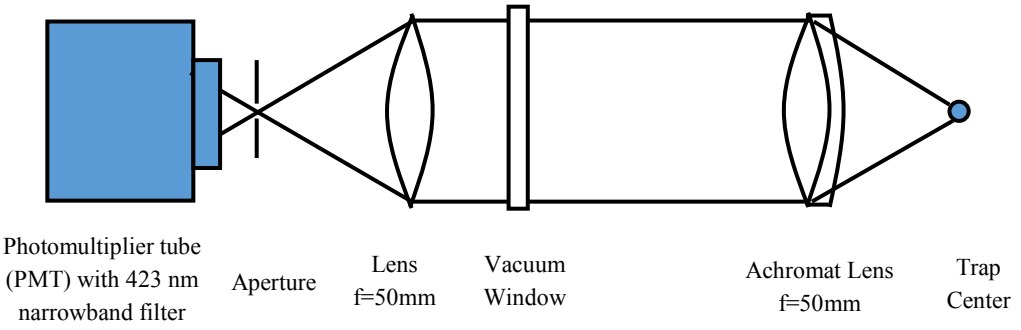

Figure 2.2 Optical system used to collect fluorescence data. The achromatic lens reduces aberrations in imaging, while the aperture minimizes scattered light from the rest of the chamber.

the field coils, as well as our characterization of the magnetic field uncertainty.

2.7 Fluorescence Lens Setup

Optimizing the 2-D MOT relies on taking fluorescence measurements to establish how many atoms are in the main chamber. We have used laser induced fluorescence in past experiments to collect information about the atoms, including spatial and velocity profiles. Two low f-number ($f/2$) achromatic lenses collect fluorescence from the atoms in the trap, each operating as shown in Fig. 2.2. Each lens is located under vacuum one focal length away from the trap center, which creates a collimated beam out of the window. Since the lens is achromatic, it minimizes both chromatic and spherical aberration in light from the trap. We coat the mounting tubes with a carbon based film to minimize stray reflections. A second, paired achromatic lens outside the chamber refocuses the beam on to a photomultiplier tube (PMT) for data collection. An aperture placed at the focal plane ensures that only light passing through the trap center is transmitted through the lens on to the PMT, while a narrow bandpass filter allows us to select fluorescence from either the calcium or the ytterbium atoms exclusively.

Chapter 3

Results and Conclusions

This chapter details the creation of the 2-D magneto-optical trap (MOT) and absorption measurements used to characterize it. We observe a maximum atomic density of 1.0×10^9 atoms/cm^3 in the 2-D MOT. In Sec. 3.3, we present a model for atomic flux from the 2-D MOT, which suggests that we should be able to achieve flux of 5×10^{10} atoms/second and load 5×10^8 atoms from the 2-D MOT into a 3-D MOT. However, we encountered significant difficulty in producing a 3-D MOT based on our calcium source, and ultimately decided to replace the 2-D MOT calcium source. Sections 3.4 and 3.5 detail these conclusions and the steps we will take in further work.

3.1 Creation of the 2-D MOT

After completing the optical setup, we produced a 2-D MOT and observed it as a fluorescent dot in the center of the MOT cross. A picture of the completed setup and a detail of the MOT fluorescence are both shown below in Fig. 3.1. Slight changes in the quarter-wave plates and laser detuning would cause the area of fluorescence to shear, deform, and eventually disappear. At the roughest level, we optimize the appearance of the 2-D MOT fluorescence to make it bright, circular, and centered in the MOT region. The MOT is most clearly visible at a laser detuning of 80 MHz.

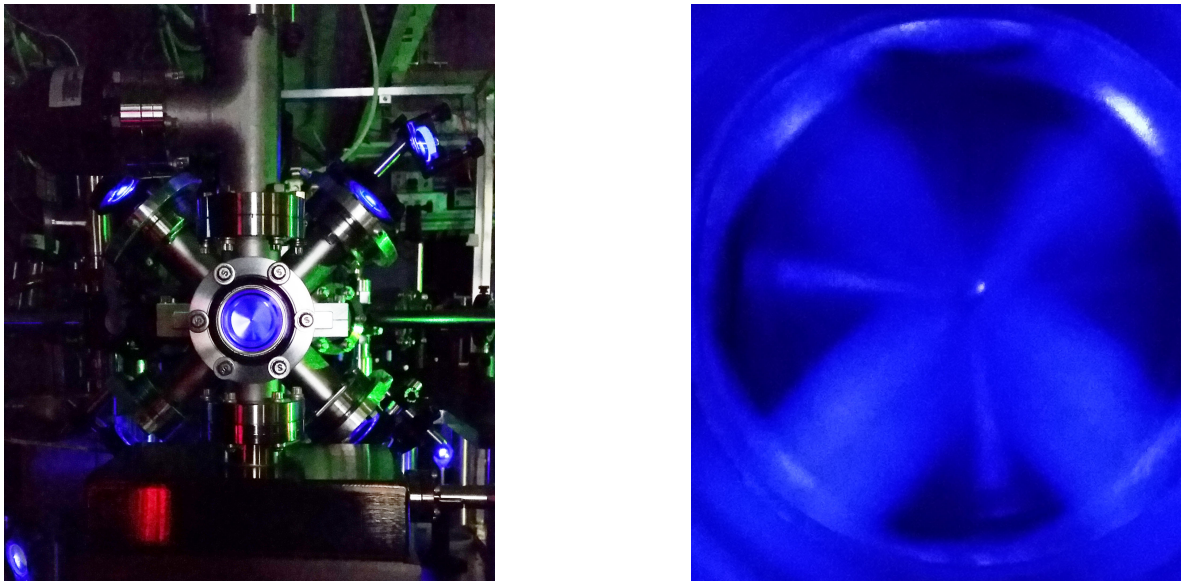

Figure 3.1 A picture of the 2-D MOT setup (left), and a zoomed in picture of the 2-D MOT fluorescence (right). The small dot in the picture on the right corresponds to the small region over which Zeeman shifts in the energy are smaller than the linewidth of the atomic transition, allowing us to estimate that the 2-D MOT has a radius of about one millimeter. The laser beams are visible as a cross since some of the hot flux in these beams fluoresces as it passes through.

3.2 Absorption Measurements of the 2-D MOT

At low intensities, the attenuation I/I_0 for a resonant beam passing through a dilute gas is given by $I/I_0 = \exp(-nl\sigma)$, where the absorption cross section $\sigma = 3\lambda^2/2\pi$ [4]. Setting up the probe beam to pass directly through the 2-D MOT, we observed an attenuation $I/I_0 = 0.895 \pm 0.04$. Assuming a trap length of 1 cm, this gives a trapped atomic density of 1.3×10^8 per cm^3. To improve this density, we doubled the beam size and rearranged the mirrors to use only the same laser beam for all four MOT beams, increasing laser power. Per Eq. (2.3), this increase in beam size requires a decrease in magnetic field gradient, so we spread the magnets farther apart to compensate. With this modified setup, we see a maximum attenuation of $I/I_0 = 0.316 \pm 0.07$. Although the beam sizes are larger, clipping from the mirrors ends up leaving the beams only about 1.4 cm wide along the axis. With the other parameters the same as above, and based on our transmission measurements, we calculate an improved atomic density of ~1×10^9 per cm^3.

3.3 Model for Atomic Flux from the 2-D MOT

Though we do not yet observe a 3-D MOT, we can use the data from our absorption measurements to determine available flux for recapture. We estimate the flux Φ of atoms accelerated out of the 2-D MOT as $\Phi = nvA$, where n is the density, v is the velocity of the atoms after push beam acceleration, and A is the cross sectional area of the 2-D MOT. Assuming a nominal radius of 0.5 mm for the 2-D MOT and 15 m/s, or one linewidth Doppler shift, for the velocity of exiting atoms, we predict a flux of 5×10^{10} atoms/second. However, this is a very simple model for the atomic flux that does not address all relevant processes. In particular, if not enough atoms enter the MOT to match the axial acceleration of atoms out of the MOT, the flux will be reduced. Tiecke, who was able to fully characterize the lithium source, reports a maximum flux of about 3×10^9 atoms/second [5].

The number of atoms that end up in the 3-D MOT depends on a balance of loading and loss mechanisms. Given the number of atoms in the beam N_b and the number of atoms in the trap N_t, we can express this relation as

$$\frac{dN_t}{dt} = \alpha N_b - \beta N_t, \tag{3.1}$$

where α and β are trap loading and loss rates. Tiecke reports that one third of the flux from his 2-D MOT is successfully recaptured [5]; assuming similar performance, we write $\alpha N_b = (\frac{1}{3})5 \times 10^{10}$ atoms/second. In our past work with ultracold plasma, we have observed that the 3-D MOT has about a 30 ms lifetime, corresponding to $\beta = 1/\tau \approx 30$ s^{-1}. When the trap is fully loaded, loss and loading mechanisms in Eq. (3.1) will balance and the number of trapped atoms will be static. Hence, we estimate the maximum number of atoms in the trap would be $N_t = \alpha N_b/\beta \approx 5 \times 10^8$. This represents an improvement of a factor of 25 over our old trap described in Sec. 1.4, which had about 2×10^7 atoms.

However this depends critically on a large input flux, which we have not been able to observe directly. Despite observing a lower loading rate than our predicted rate, Tiecke was still able to load up to 10^{10} atoms in his trap [5]. This indicates a much lower value for the loss rate β in his experiment, perhaps because there is no background flux in the main chamber. Hence even if the flux achieved from our 2-D MOT is much lower than expected, it could likely still support a MOT size on the order of 10^8 or 10^9 atoms.

3.4 Conclusions

To summarize, we demonstrate that a 2-D MOT is feasible for calcium. However, we were not able to successfully use the 2-D MOT source to load a 3-D MOT in our main chamber. We suspect that a slight misalignment of the 2-D MOT beams can deflect atoms as they leave the trap, even after removing the differential pumping channel between the 2-D MOT and the main chamber. Based on

calcium's photon recoil (the velocity change corresponding to a single atom-photon interaction) of 2.5 cm/s, the geometry of our chamber, and the velocity of atoms leaving the 2-D MOT (15 m/s), we calculate that six photon recoils would prevent the atoms from reaching the capture region of the 3-D MOT. Observing our beam quality and divergence, we are fairly certain we cannot achieve this level of precision without investing considerable amounts of money for improving our laser system. As such, we have decided to replace our 2-D MOT with a traditional Zeeman slower. While this will once again introduce hot background flux, we are confident that it will allow us to push forward more quickly with our experiment.

3.5 Directions for Further Work

When we achieve a 3-D MOT, we intend to systematically vary 2-D MOT laser detuning and power, oven temperature, and push beam power to produce maximum loading into the 3-D MOT. We will analyze fluorescence data to determine the number of atoms trapped in the main chamber, and compare with our estimates to determine our trapping efficiency.

Immediately after creating a 3-D MOT, we intend to measure several transition frequencies in calcium. The modifications we describe in Sec. 2.6 reduce systematic bias in measured frequencies due to the background magnetic field to about 100 kHz. With the other precision spectroscopy tools in our lab, we expect to be able to make measurements with an additional uncertainty of less than 100 kHz. Since this work only requires a calcium MOT, we can conduct these measurements while still developing our ytterbium MOT.

Once we are able to load both calcium and ytterbium into the trap, we will form a dual-species MOT . Since our main research thrust is in ultracold plasma, we will use this new setup to study energy relaxation in a dual species plasma. In past work, we have characterized expansion rates of a calcium ultracold neutral plasma in great detail. By introducing a ytterbium plasma in the

expanding calcium plasma, we will strongly perturb the system and observe the resulting effect on the calcium ions' energy and expansion. By staggering the time between the calcium and ytterbium plasma formation and the relative density of each species, we will be able to probe these interactions in great detail.

The dual species MOT will also enable us to study other important strongly coupled systems, as well as CaYb molecular formation rates. With these varied applications in mind, we are confident that our dual-species MOT will be a rich testing ground for a variety of interesting physics.

Appendix A

Power Switching Electronics

As we explained in Sec. 2.6, performing high-precision measurements on the trapped atomic species necessitates not only canceling the background magnetic field, but also quickly switching off the MOT quadrupole field.

We based the design of the magnetic field coils and related electronics on a paper by Streed et al., which allows us to quickly switch off coil power and dissipate the magnetic field [10]. Figure A.1 shows a schematic for the power supply switch. An integrated gate bipolar transistor (IGBT) quickly shuts off current in the power lines, and a high current diode protects the setup from voltage spikes. During steady operation, both elements emit about 400 W through Joule heating, and hence require water cooling.

A secondary "debounce" circuit shorts out the magnetically induced emf immediately after switching and then dissipates the remaining energy. A varistor, which has high resistance at low voltages but whose resistance drops precipitously at high voltage, clamps voltage across the coils. Even as current continues to rise, the voltage across the varistor will not exceed its maximum rating, protecting other elements in the system from electric shocks. When the inductive emf has subsided to lower values, current passes through the diode-resistor combination, dissipating the remaining inductive energy.

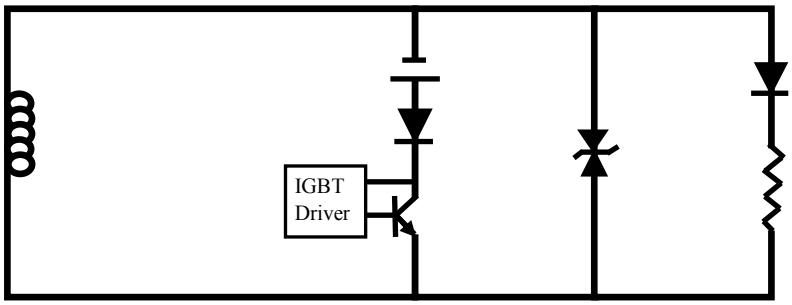

Figure A.1 Circuit schematic for magnetic field dissipation. A high current diode in series with the power supply (center) protects it from high voltage shocks. The IGBT allows quick switching of power, with rise and fall times 300 ns. The inductive load (coils, at left) will produce a sharp voltage peak which shorts through the varistor. A short time later, the remaining energy dissipates through the resistor at the far right.

Even though our electronics permit fast switching of the magnetic field coils (with rise and fall times of 190 and 350 ns), the field does not immediately disappear. As power leaves the system, the magnetic field will exponentially decay with characteristic time constant $\tau = L/R$, where L is the inductance of the load and R is the value of the resistor. We measured the inductance of the coils as $L = 0.96 \pm 0.3\mu$H, while the resistor has resistance of $R = 1\Omega$, such that $\tau \approx 1\mu s$ After five time constants, the magnetic field in the region of the trap will have decreased to around 0.5 G/cm. Atoms expanding ballistically from the trap will have a velocity of about 1 m/s, which on this time scale will allow them to travel 5 μm. This distance is minimal in comparison to the trap radius $r \approx 1$ mm, and hence will neither increase the Zeeman shift nor decrease the fluorescence signal. Atoms will be subject to a field of about 0.05 gauss at the edge of the trap. Since the Bohr magneton μ_B equals 1.4 MHz/G, the leftover field will introduce an additional uncertainty of 70 kHz into our frequency measurements.

Bibliography

[1] L. D. Carr, D. DeMille, R. V. Krems, and J. Ye, "Cold and ultracold molecules: science, technology and applications," New Journal of Physics **11,** 055049 (2009).

[2] Plasma Science Committee and Plasma 2010 Committee, *Plasma Science: Advancing Knowledge in the National Interest (Physics 2010)* (National Academies Press, Washington, D.C., 2007).

[3] G. Bannasch, J. Castro, P. McQuillen, T. Pohl, and T. Killian, "Velocity Relaxation in a Strongly Coupled Plasma," Physical Review Letters **109,** 185008 (2012).

[4] H. J. Metcalf and P. Van der Straten, *Laser cooling and trapping* (Springer, 1999).

[5] T. Tiecke, S. Gensemer, A. Ludewig, and J. Walraven, "High-flux two-dimensional magneto-optical-trap source for cold lithium atoms," Physical Review A **80,** 013409 (2009).

[6] T. G. Tiecke, "Feshbach resonances in ultracold mixtures of the fermionic quantum gases 6Li and 40K," Ph.D. dissertation (University of Amsterdam, Amsterdam, Netherlands, 2009).

[7] A. Ridinger, S. Chaudhuri, T. Salez, U. Eismann, D. R. Fernandes, K. Magalhaes, D. Wilkowski, C. Salomon, and F. Chevy, "Large atom number dual-species magneto-optical trap for fermionic 6 Li and 40 K atoms," The European Physical Journal D-Atomic, Molecular, Optical and Plasma Physics **65,** 223–242 (2011).

[8] S. Dörscher, A. Thobe, B. Hundt, A. Kochanke, R. Le Targat, P. Windpassinger, C. Becker, and K. Sengstock, "Creation of quantum-degenerate gases of ytterbium in a compact 2D-/3D-magneto-optical trap setup," Review of Scientific Instruments **84,** 043109 (2013).

[9] M. Lyon and S. Bergeson, "Precision spectroscopy using a partially stabilized frequency comb," Applied Optics **53,** 5163–5168 (2014).

[10] E. W. Streed, A. P. Chikkatur, T. L. Gustavson, M. Boyd, Y. Torii, D. Schneble, G. K. Campbell, D. E. Pritchard, and W. Ketterle, "Large atom number Bose-Einstein condensate machines," Review of Scientific Instruments **77,** 023106 (2006).

Index